SURFACE BIFURCATION IN ANISOTROPIC MATERIALS WITH APPLICATION TO ALUMINUM ALLOYS

by:

M. D. NESTOROVIĆ, E. CHU and N. TRIANTAFYLLIDIS

Published in the: Journal of Applied Mechanics, 1999, Volume 66, pp.62-68

SURFACE BIFURCATION IN ANISOTROPIC MATERIALS WITH APPLICATION TO ALUMINUM ALLOYS

by:

M. D. NESTOROVIĆ, E. CHU† and N. TRIANTAFYLLIDIS

Department of Aerospace Engineering
The University of Michigan
Ann Arbor, Michigan 48109-2140

† Product Manufacturing Engineering
ALCOA Technical Center
Alcoa Center, Pennsylvania 15069-0001

Abstract

Surface bifurcation is an instability mechanism which appears in the form of surface waviness on traction-free surfaces in ductile solids subjected to large strains. In sheet metal forming, the practical interest in this phenomenon stems from the fact that it occurs past the onset of localization, i.e. the forming limit, but prior to the local fracture failure in a quasi-static, monotonic loading process. In this work, we apply the general theory for surface bifurcation in a homogeneously strained, anisotropic, rate-independent, elastoplastic half-space, to study the influence of material anisotropy on the onset of surface instabilities. In particular, we calculate the critical principal strains $\varepsilon_1^c, \varepsilon_2^c$ and the corresponding eigenmode orientation angle Ω_c when the principal strain axes are at a fixed angle α with respect to the rolling direction of the solid.

The presented calculations are for a 2024-T3 aluminum alloy, whose constitutive properties have been determined experimentally. It is found that by varying the strain orientation angle α, the surface bifurcation strains can vary up to an order of 80% for in-plane principal strains of a different sign, but only up to an order of 10% for principal strains of the same sign. The eigenmode orientation angle Ω_c is calculated for a particular strain orientation ($\alpha = \pi/6$), for which case it is found that Ω_c is close to the forming limit angle ψ_c only for positive principal strains. The presentation is concluded by a discussion of the influence of the anisotropy and the yield surface parameters of the constitutive model on surface bifurcation.

1 Introduction and Motivation

An instability phenomenon occurring during a quasi-static loading of ductile solids at adequately high levels of strain, is the development of surface waviness on the previously smooth traction-free boundaries. The resulting surface roughness is in the form of same orientation surface wrinkles of a very short wavelength. Upon further straining, the development of microcracks at the bottom of the wave troughs, which eventually leads to fracture, justifies the interest in surface bifurcation as a precursor phenomenon to the ultimate failure by fracture.

The credit for the theoretical explanation of this phenomenon within the context of large strain continuum mechanics goes to Biot (1965), who was the first to show the possibility of a bifurcation instability occurring in an elastic, traction-free half-space subjected to large in-plane stresses. The corresponding eigenmode decays exponentially away from the surface, but the analysis provides no characteristic wavelength for the mode. Subsequent investigations at large deformations in finite size elastoplastic solids showed that surface bifurcations always appear on the free surfaces after an adequate amount of straining in compression as well as in tension. Examples of surface bifurcations in structures include the elastoplastic rectangular block under tension and compression by Hill and Hutchinson (1975) and Young (1976) respectively, the pure bending of elastic and elastoplastic rectangular bars by Triantafyllidis (1980) and the internal pressurization of cylindrical tubes by Larsson *et al* (1982). It should be emphasized at this point that the roughness resulting from a bifurcation, and which appears at high levels of strain in the form of similarly oriented wavelets, is due to the interaction between the finite strain kinematics and the nonlinearity of the constitutive law. This phenomenon should not be confused with the surface roughness which can appear at any initially smooth surface and which grows linearly with strain in the small strain regime, in the form of "*orange peel*" with no preferred orientation observed. The latter phenomenon is due to the orientation mismatch of the surface grains in metal polycrystals and requires micromechanical descriptions of the solid at the grain level, as the interested reader can see from the recent work by Becker (1997).

The critical load at surface bifurcation is strongly dependent on the constitutive model as well as on the in-plane stress state. For isotropic, incompressible, rate-independent solids, Hutchinson and Tvergaard (1980) have studied the surface bifurcation of a traction-free half-space under proportional straining conditions, using a finite strain generalization of the J_2 deformation theory of plasticity. Their analysis is capable of finding the lowest strain surface bifurcation only for isotropic solids, due to a particular form assumed for the eigenmode. In a subsequent work, Triantafyllidis (1984) presented the general analysis for the surface bifurcation in any anisotropic, rate-independent, traction-free half-space. The latter work

investigates all the possible modes in order to find the wanted critical load. In the same work it is shown that the bifurcation mode is polarized along a certain direction, i.e. it consists of waves whose crests are parallel lines, exactly as observed in experiments involving approximately homogeneous principal strain fields as in the case of bending of bars or bursting of internally pressurized tubes (see the corresponding pictures in Hutchinson and Tvergaard (1980) and Larsson *et al* (1982)).

The present work is motivated by problems in sheet metal forming involving alloys subjected to finite strain and for which a high quality of the finished surface is required. Since the alloys in question are in general anisotropic, the investigation of surface bifurcation requires the general methodology given by Triantafyllidis (1984). Of particular interest is the influence of anisotropy, measured by the angle α formed between the principal strains and the rolling direction, on the surface bifurcation. All the corresponding calculations are based on the recently proposed anisotropic plasticity theories by Karafillis and Boyce (1993). The numerical results presented in this work correspond to a particular aluminum alloy 2024-T3 whose material properties have been determined experimentally by Barlat *et al* (1991).

Results are presented for three different values of the principal strain orientation angle α and show a strong influence of plastic anisotropy on the critical strains for principal strains of a different sign. The eigenmode orientation angle Ω_c is also calculated as a function of the principal strain ratio $\tan\varphi$ for a particular value of the principal strain orientation angle α. Finally, to study the influence of the yield surface, the critical strains for the anisotropic material are compared to their counterparts of two fictious isotropic materials, both with the same uniaxial stress-strain curve in the rolling direction as the alloy under investigation.

2 General Theory for Surface Bifurcation

The general theory for the surface bifurcation of a traction-free half-space, consisting of an anisotropic, homogeneous, rate-independent material, which is subjected to a homogeneous, in-plane state of stress, has been derived by Triantafyllidis (1984). However, for reasons of completeness, a brief outline of this theory is presented here.

In the current configuration, a Cartesian coordinate system is used, in which the solid occupies the half-space $x_3 \leq 0$. An updated Lagrangian formulation of the problem is presented, with Δf denoting the perturbation of any field quantity from the spatially constant principal solution whose uniqueness is under investigation. The perturbed equilibrium equations and the traction-free surface boundary conditions are expressed in terms of the first Piola-Kirchhoff stress $\mathbf{\Pi}$ as follows

$$\Delta \Pi_{ij,i} = 0 \qquad (x_\alpha \in \Re,\ x_3 \leq 0)^1 \tag{1}$$

$$\Delta \Pi_{3i} = 0 \qquad (x_\alpha \in \Re,\ x_3 = 0). \tag{2}$$

For any rate-independent material, the perturbation of the first Piola-Kirchhoff stress is related to the perturbation of the deformation gradient $\mathbf{F}$ by the linearized constitutive relation

$$\Delta \Pi_{ji} = L_{ijkl} \Delta F_{kl} \tag{3}$$

$$\Delta F_{kl} = \Delta u_{k,l} \tag{4}$$

where $\Delta \mathbf{u}$ is the perturbation of the displacement.

The incremental moduli tensor $\mathbf{L}$ is a function of the material properties and the current state of stress. Explicit expressions for the case of some finitely strained aluminum alloys will be given in the next section. At this point it suffices to say that the half-space is assumed homogeneous, incrementally linear and under a spatially constant state of stress which has been achieved through a given strain history. The loading path in question is parameterized by a "*time-like*" scalar λ which increases monotonically from zero and is assumed to uniquely characterize the present state of the material. Consequently the components of the incremental moduli tensor are λ-dependent constants $L_{ijkl}(\lambda)$.

[1] Here and subsequently, Latin indexes range from 1 to 3, while Greek indexes range from 1 to 2. Einstein's summation convention is implied over repeated indexes. Repeated indexes in parentheses are not summed, unless indicated explicitly.

The governing equations (1), (3), (4) and the boundary conditions (2) have to be complemented by the requirement of bounded displacement and deformation gradient perturbations, which in addition must decay to zero away from the surface, i.e.

$$\Delta u_i \to 0, \qquad \Delta F_{ij} \to 0, \qquad \text{as} \;\; x_3 \to -\infty. \tag{5}$$

The above system of linear partial differential equations with constant coefficients can be reduced to a system of ordinary differential equations in x_3 by considering its Fourier transform with respect to x_α. By substituting the constitutive (3) and kinematic equations (4) into the equilibrium equations (1) and subsequently considering the Fourier transform of the resulting equations with respect to x_α, we obtain the following system of ordinary differential equations in x_3

$$(i\omega_\alpha)(i\omega_\beta)L_{i\alpha k\beta}\Delta\hat{u}_k + (i\omega_\gamma)(L_{i3k\gamma} + L_{i\gamma k3})\Delta\hat{u}_{k,3} + L_{i3k3}\Delta\hat{u}_{k,33} = 0 \tag{6}$$

where $\Delta\hat{u}_k(\omega_\alpha, x_3)$ is the double Fourier transform of $\Delta u_k(x_\alpha, x_3)$, with ω_α the Fourier transform variable corresponding to x_α. In deriving (6) it is tacitly assumed that the perturbation fields Δu_k are adequately smooth (at least twice continuously differentiable) and uniformly bounded with respect to all coordinates. The boundedness requirement for Δu_k implies that the Fourier transforms $\Delta\hat{u}_k$ are not functions of their arguments in the classical sense, but distributions in the ω_α plane.

The general solution to the system of ordinary differential equations with constant coefficients in (6) is found to be the sum of three linearly independent partial solutions

$$\Delta\hat{u}_k(\omega_\alpha, x_3) = \sum_{j=1}^{3} \xi_{(j)}(\omega_\alpha) A_k^{(j)} \exp[i\omega z_{(j)} x_3] \tag{7}$$

where the following notations have been employed: The quantity ω is the norm of the vector ω_α (i.e. $\omega \equiv |\omega_\alpha\omega_\alpha|^{1/2}$) and $z_{(j)}$ denote the three roots with negative imaginary part of the following sixth order polynomial in z

$$\det[L_{i\alpha k\beta}n_\alpha n_\beta + (L_{i3k\gamma} + L_{i\gamma k3})n_\gamma z + L_{i3k3}z^2] = 0 \tag{8}$$

where $\omega_\alpha = \omega n_\alpha$, $n_1 = \cos\Omega$, $n_2 = \sin\Omega$ and $z_{(j)} = a_{(j)}(\Omega, \lambda) + ib_{(j)}(\Omega, \lambda)$ such that $b_{(j)} < 0$ (j = 1–3).

The requirement that for the load parameter λ values of interest no real roots of (8) are allowed for any angle Ω, stems from the fact that we seek surface instabilities occurring in the elliptic regime of the material response, i.e. prior to the occurrence of any localized mode of deformation. Recall (e.g. Rice (1976)) that the mathematical expression for the strong ellipticity condition is $L_{ijkl}(\lambda)n_j n_l > 0$ for all three-dimensional unit vectors $\mathbf{n}$, which implies the necessity of non-real roots for (8). The selection of

the three roots of the sixth order polynomial in (8) which have a negative imaginary part, follows from (5) which requires the perturbation to decay away from the free surface. The unit vector $\mathbf{A}^{(j)}$, which is associated with the root $z_{(j)}$ is the eigenvector of the following 3×3 matrix

$$[L_{i\alpha k\beta} n_\alpha n_\beta + (L_{i3k\gamma} + L_{i\gamma k3}) n_\gamma z_{(j)} + L_{i3k3} z_{(j)}^2] A_k^{(j)} = 0. \tag{9}$$

For a simple root $z_{(j)}$, the corresponding eigenvector $\mathbf{A}^{(j)}$ in (9) is unique, while for a double root, one has two corresponding eigenvectors which are chosen to be mutually orthogonal[2]. Finally, $\xi_{(j)}(\omega_\alpha)$ is the amplitude of the j-th partial solution $A_k^{(j)} \exp[i\omega z_{(j)} x_3]$ and is a distribution defined in the Fourier transform space ω_α to be specified subsequently.

The Fourier transform of the surface boundary conditions (2), after substituting the constitutive (3) and kinematic equations (4) and the general expression for the transform of the displacement perturbation in (7), gives the following result

$$\sum_{j=1}^{3} S_{ij}(\Omega, \lambda) \xi_{(j)}(\omega_\alpha) = 0, \qquad S_{ij}(\Omega, \lambda) \equiv [L_{i3k\alpha}(\lambda) n_\alpha + L_{i3k3}(\lambda) z_{(j)}] A_k^{(j)}. \tag{10}$$

For the homogeneous system in (10) to admit a non-trivial solution $\xi_{(j)}(\omega_\alpha)$, the matrix of constants S_{ij} must be singular. Thus, onset of the surface bifurcation corresponds to the first such occurrence of a singular matrix S_{ij} (at a load level λ_c and for an angle Ω_c), as the load parameter λ increases from zero. Hence

$$\begin{aligned} &\det[S_{ij}(\Omega_c, \lambda_c)] = 0; \\ &\det[S_{ij}(\Omega, \lambda)] \neq 0, \text{ for } \Omega \in [0, \pi) \text{ and } 0 \leq \lambda < \lambda_c. \end{aligned} \tag{11}$$

Note that in the above procedure of searching for the critical load λ_c, only the domain $[0, \pi)$ has to be scanned for Ω, at each increment of λ. Indeed from (8), one obtains that $z_{(j)}(\Omega + \pi) = -z_{(j)}(\Omega)$, which will result in the equivalent condition $\det[\overline{S}_{ij}(\Omega_c, \lambda_c)] = 0$ at criticality.

At this point we present an important remark about the shape of the eigenmode. For the homogeneous system in (10), to admit at λ_c a non-trivial solution in the ω_α plane, the corresponding eigenmode $\xi_{(j)}$ should vanish in all points except those along the direction $\omega_2/\omega_1 = \tan\Omega_c$. In this case the distribution $\xi_{(j)}(\omega_\alpha)$ has a line support along the above mentioned direction, i.e.

$$\xi_{(j)}(\omega_\alpha) = \Xi_{(j)} f, \qquad \text{supp} f = \{\omega_\alpha \mid \omega_2/\omega_1 = \tan\Omega_c\} \tag{12}$$

[2]This choice is always possible in the case where the moduli have the major symmetry $L_{ijkl}(\lambda) = L_{klij}(\lambda)$, a condition met in all plasticity theories leading to self adjoint problems.

where $\Xi_{(j)}$ is a unit vector obtained from (10), at λ_c, Ω_c and f is a scalar distribution in the Fourier plane ω_α, with a line support indicated in (12). It follows from (12) and (7) that upon inversion of the Fourier transform for the perturbed displacement one obtains

$$\Delta u_k(x_1, x_2, x_3) = \Delta u_k(x_1 \cos\Omega_c + x_2 \sin\Omega_c, x_3), \tag{13}$$

i.e. the bifurcation eigenmode is in the form of waves polarized along the direction $\tan\Omega_c$, which is graphically represented in Figure 1. The amplitude of these waves as well as their shape cannot be specified by this analysis in view of the arbitrariness of the distribution f in (12).

To complete the general theory, one needs to specify the loading path followed from the stress-free configuration. An in-plane stress state is required, which dictates that the Kirchhoff stress[3] components on the free surface vanish, namely

$$\tau_{3i}(\lambda) = 0. \tag{14}$$

The stress state in the half-space is achieved through a proportional straining path, where the in-plane principal logarithmic strains ε_α are oriented at a fixed angle α with respect to the x_i material axis of orthotropy and have a constant ratio $\tan\varphi$, i.e.

$$\varepsilon_1 = \lambda\cos\varphi, \qquad \varepsilon_2 = \lambda\sin\varphi \tag{15}$$

while the in-plane components of the strain rate tensor $D_{\alpha\beta}$ are given by

$$D_{\alpha\beta} = \begin{bmatrix} \cos\alpha & -\sin\alpha \\ \sin\alpha & \cos\alpha \end{bmatrix} \begin{bmatrix} \cos\varphi & 0 \\ 0 & \sin\varphi \end{bmatrix} \begin{bmatrix} \cos\alpha & \sin\alpha \\ -\sin\alpha & \cos\alpha \end{bmatrix}. \tag{16}$$

From the above relations (14)-(16) for the loading path, one can calculate the stress state $\boldsymbol{\tau}(\lambda)$ and consequently the incremental moduli $\mathbf{L}(\lambda)$ in (3) which are given as functions of the current stress state. The functional dependence $\mathbf{L}(\boldsymbol{\tau})$ depends on the constitutive model adopted and a specific selection for aluminum alloys will be proposed in the next section. At this point it suffices to say, that for finitely strained elastoplastic solids a convenient form of the constitutive law is given by the incremental moduli tensor $\boldsymbol{\mathcal{L}}(\boldsymbol{\tau})$ which relates the Jaumann rate of the Kirchhoff stress $\overset{\nabla}{\boldsymbol{\tau}}$ to the strain rate tensor $\mathbf{D}$. In the absence of a rigid body rotation of the solid, $\overset{\nabla}{\boldsymbol{\tau}} = d\boldsymbol{\tau}/d\lambda$, and hence

$$\frac{d\tau_{ij}}{d\lambda} = \mathcal{L}_{ijkl}(\boldsymbol{\tau}(\lambda))D_{kl}. \tag{17}$$

[3]Use of the Kirchhoff stress measure leads to the incremental moduli $\mathbf{L}$ with the major symmetry $L_{ijkl} = L_{klij}$ if the same symmetry is adopted for the incremental moduli $\boldsymbol{\mathcal{L}}$.

From (17) the relations between the known constant strain rates $D_{\alpha\beta}$ and the non-zero stress rate components are

$$\frac{d\tau_{\alpha\beta}}{d\lambda} = \mathcal{P}_{\alpha\beta\gamma\delta}(\boldsymbol{\tau}(\lambda))D_{\gamma\delta}, \qquad \mathcal{P}_{\alpha\beta\gamma\delta} \equiv \mathcal{L}_{\alpha\beta\gamma\delta} - \frac{\mathcal{L}_{\alpha\beta 33}\mathcal{L}_{33\gamma\delta}}{\mathcal{L}_{3333}}. \tag{18}$$

In deriving the plane stress incremental equations in (18) it is tacitly assumed that x_3 is a material axis of orthotropy, a property which when combined with the plane stress assumption (14) gives for the out of plane strain rates $D_{3\alpha} = 0$, $D_{33} = -\mathcal{L}_{33\gamma\delta}D_{\gamma\delta}/\mathcal{L}_{3333}$ and hence the expressions for the plane stress moduli $\boldsymbol{\mathcal{P}}(\boldsymbol{\tau})$ recorded in (18).

The determination of the stress state $\boldsymbol{\tau}(\lambda)$ from (16) and (18) leads to the calculation of the complete moduli tensor $\boldsymbol{\mathcal{L}}(\boldsymbol{\tau})$ from which one can find the moduli tensor $\mathbf{L}(\lambda)$, required by the general analysis in (3) to be

$$L_{ijkl} = \mathcal{L}_{ijkl} - \frac{1}{2}(\tau_{ik}\delta_{jl} + \tau_{il}\delta_{jk} + \tau_{jk}\delta_{il} - \tau_{jl}\delta_{ik}). \tag{19}$$

The above result follows from the definitions of the moduli $\mathbf{L}$ ($d\Pi_{ji}/d\lambda = L_{ijkl}(\lambda)(dF_{kl}/d\lambda)$) and $\boldsymbol{\mathcal{L}}$ in (17), the relations between the two stress measures $(\boldsymbol{\Pi},\boldsymbol{\tau})$ and their work conjugate strain rate measures $(d\mathbf{F}/d\lambda, \mathbf{D})$, and is a straightforward calculation in continuum mechanics. The above discussion gives the physical meaning of the time-like parameter λ as a measure of the principal strain size (see (15)) and provides an explicit methodology for the determination of the moduli $\mathbf{L}(\lambda)$ which enter the calculations for the onset of the surface bifurcation.

3 Constitutive Model

As mentioned above, the application of the general surface bifurcation analysis to a specific solid requires the material properties of the solid, which enter through the incremental moduli tensor $\boldsymbol{\mathcal{L}}(\boldsymbol{\tau})$ that relates the Jaumann rate of the Kirchhoff stress $\overset{\nabla}{\boldsymbol{\tau}}$ to the strain rate tensor $\mathbf{D}$. For buckling problems in metals, which occur during a proportional loading path, as is the case here, it has been established that the deformation theory of plasticity gives better correlation to experiments, as compared to the standard flow theory with a smooth yield surface (see the review article by Hutchinson (1974)). Following Stören and Rice (1975), an attractive way to obtain a finite strain version of the deformation theory of plasticity is by assuming that the incremental moduli, derived for deformation theory under a small strain assumption, are also the ones relating the Jaumann rate of the Kirchhoff stress to the strain rate. Their method, which also assumed a von Mises isotropic yield function $\Phi(\boldsymbol{\tau})$, was applied to the prediction of the forming limit diagrams of biaxially stretched metallic sheets. The generalization of this model for the case of anisotropic yield functions $\Phi(\boldsymbol{\tau})$, which has been used by Triantafyllidis and Needleman (1980) for wrinkling calculations in the cup drawing test, is adopted for our purpose and has the following incremental moduli tensor $\boldsymbol{\mathcal{L}}(\boldsymbol{\tau})$ components

$$\mathcal{L}_{ijkl} = Q^{-1}_{ijkl} - \frac{[Q^{-1}_{ijmn}(\partial\tau_e/\partial\tau_{mn})][(\partial\tau_e/\partial\tau_{pq})Q^{-1}_{pqkl}]}{[(E_t)^{-1} - (E_s)^{-1}]^{-1} + [(\partial\tau_e/\partial\tau_{pq})Q^{-1}_{pqrs}(\partial\tau_e/\partial\tau_{rs})]} \tag{20}$$

$$Q_{ijkl} = \frac{1+\nu}{E}[\frac{1}{2}(\delta_{ik}\delta_{jl} + \delta_{il}\delta_{jk}) - \frac{\nu}{1+\nu}\delta_{ij}\delta_{kl}] + (\frac{1}{E_s} - \frac{1}{E})(\frac{\partial\tau_e}{\partial\tau_{ij}}\frac{\partial\tau_e}{\partial\tau_{kl}} + \frac{\partial^2\tau_e}{\partial\tau_{ij}\partial\tau_{kl}}). \tag{21}$$

In the above expressions, E is the Young's modulus, ν the Poisson's ratio of the material's uniaxial response and $\tau_e(\boldsymbol{\tau})$ is the effective stress (τ_e is a function of Φ) which is a homogeneous function of $\boldsymbol{\tau}$, of degree one. In addition, $E_s(\tau_e)$ and $E_t(\tau_e)$ are the secant and tangent moduli evaluated at a stress level τ_e on the uniaxial stress-strain curve. Finally, the rank four tensor $\mathbf{Q}^{-1}$ is the inverse of $\mathbf{Q}$ in (21) and is assumed to have the same symmetries as $\mathbf{Q}$, i.e. $Q_{ijpq}Q^{-1}_{pqkl} = (1/2)(\delta_{ik}\delta_{jl} + \delta_{il}\delta_{jk})$ and $Q^{-1}_{ijkl} = Q^{-1}_{klij} = Q^{-1}_{jikl} = Q^{-1}_{ijlk}$. It should also be mentioned that the moduli in (20) and (21) assume loading of the solid in the plastic regime of the response, i.e. $\tau_e \geq \tau_y$, where τ_y is the yield stress.

The above proposed formulation is applicable to anisotropic rate-independent elastoplastic materials which do not exhibit the Bauschinger effect, i.e. materials which exhibit no difference between their tensile and compressive responses. Instead of expressing the equivalent stress τ_e, or the yield function Φ ($\tau_e = (\Phi/2)^{1/m}$)[4] as anisotropic functions of $\boldsymbol{\tau}$ (e.g. Hill (1950)), Karafillis and Boyce (1993) have proposed the concept of an "*Isotropic Plasticity Equivalent*" (IPE) material, for which τ_e is an isotropic

[4] Φ is usually a homogeneous polynomial in $\boldsymbol{\tau}$ of order m. For the von Mises case $m = 2$.

function of the IPE material's stress. The IPE material's stress tensor $\mathbf{s}$ is related to the actual stress tensor $\boldsymbol{\tau}$ of the anisotropic material by a rank four symmetric tensor $\mathbf{A}$ which characterizes the anisotropy of the material. Thus, it is assumed that

$$\tau_e = \left(\frac{|s_1 - s_2|^m + |s_2 - s_3|^m + |s_3 - s_1|^m}{2} \right)^{1/m} \tag{22}$$

where s_I are the principal values of $s_{ij} = A_{ijkl}\tau_{kl}$.

The specific choice of $\tau_e(\mathbf{s})$ in (22) used here has also been employed by Barlat *et al* (1991) and was first proposed for isotropic materials by Hershey (1954). For the case of orthotropic materials, like the aluminum alloys of interest, the transformation tensor $\mathbf{A}$ contains only six independent non-zero components c_J, namely

$$\begin{aligned}
&A_{1111} = (c_2 + c_3)/3, \;\; A_{2222} = (c_1 + c_3)/3, \;\; A_{3333} = (c_1 + c_2)/3, \\
&A_{1122} = A_{2211} = -c_3/3, \;\; A_{1133} = A_{3311} = -c_2/3, \;\; A_{2233} = A_{3322} = -c_1/3, \\
&A_{2323} = A_{2332} = A_{3223} = A_{3232} = c_4/2, \\
&A_{1313} = A_{1331} = A_{3113} = A_{3131} = c_5/2, \\
&A_{1212} = A_{1221} = A_{2112} = A_{2121} = c_6/2.
\end{aligned} \tag{23}$$

In addition to the equations (20)-(23), the complete characterization of the material model requires the uniaxial stress-strain curve of the material, which is determined experimentally, as are the constant exponent m, appearing in the equivalent stress determination in (22), and the six anisotropy coefficients c_J in (23).

4 Results and Discussion

The numerical calculation of the critical load λ_c at the onset of surface bifurcation and of the corresponding eigenmode direction Ω_c proceeds as follows:

The construction of the stability matrix $S_{ij}(\Omega, \lambda)$ defined in (10), which is required for the calculation of λ_c and Ω_c according to (11), involves the determination of the current stress state $\tau_{\alpha\beta}(\lambda)$. The calculation of the stress state at load parameter λ is based on the system of first order ordinary differential equations in (18), which are numerically integrated using a second order Runge-Kutta method with a step size $\Delta\lambda = 10^{-4}$. To verify the accuracy of the numerical stress integration algorithm, the results have been compared with the known analytical solution for the special case of a von Mises isotropic material. For this isotropic material, the constitutive equations reduce to the J_2 deformation theory, i.e. the exponent in the definition of the equivalent stress τ_e in (22) is $m = 2$ and the all six coefficients in (23) which characterize the orthotropy of the material are $c_J = 1$. For this case it can be shown (e.g. Triantafyllidis *et al* (1982)) that the principal stresses τ_α are related to the principal strains ε_α by

$$\begin{aligned} \tau_\alpha &= \frac{E_s}{1-\nu_s^2}[(1-\nu_s)\varepsilon_\alpha + \nu_s(\varepsilon_1+\varepsilon_2)] \\ \nu_s &= \frac{1}{2} + \frac{E_s}{E}(\nu - \frac{1}{2}) \end{aligned} \tag{24}$$

where $E_s(\tau_e)$ is the secant modulus evaluated at the equivalent stress $\tau_e = (\tau_1^2 - \tau_1\tau_2 + \tau_2^2)^{1/2}$. When comparing the stresses obtained by the previously described numerical integration algorithm to their exact counterparts in (24), for the isotropic material case, the error in the stresses is of the order 0.1%.

The numerical determination of the critical load λ_c is based on the evaluation of the minimum value, with respect to the angle Ω, of the determinant of the stability matrix in (11) every ten load increments. The Ω minimum of the determinant is also obtained numerically by scanning the $[0, \pi)$ interval in 315 equal increments. Further verification of the accuracy of our algorithm is obtained by comparing our results with those of Hutchinson and Tvergaard (1980) for an isotropic, incompressible, rate-independent material with a hardening exponent of $n = 0.1$.

The material investigated for surface bifurcation is a 2024-T3 aluminum alloy, whose anisotropy coefficients c_J and exponent m appearing in the definition of the equivalent stress τ_e have been experimentally determined by Barlat *et al* (1991). The alloy's experimentally obtained uniaxial stress-strain response along the rolling direction ($\alpha = 0$) is fitted to a power law of the type $(\tau/\tau_y) = (\varepsilon/\varepsilon_y)^n$ or equivalently $\tau = K\varepsilon^n$ where $\tau_y = E\varepsilon_y$. The numerical values used in the calculations are summarized in Table 1 for the anisotropic yield function coefficients and the uniaxial stress-strain constants are: $E = 69000$ MPa,

Material	m	c_1	c_2	c_3	c_4	c_5	c_6
2024-T3	8	1.378	1.044	0.955	1.000	1.000	1.210

Table 1: Coefficients of the anisotropic yield function

$\nu = 0.31$, $K = 667.69$ MPa and $n = 0.114$.

The results of the calculations are plotted in the principal logarithmic strain space $\varepsilon_1 - \varepsilon_2$ in Figures 2-4 and Figure 6 with the surface bifurcation points in each figure corresponding to the solid curve. The dashed curve represents the loss of ellipticity in the three-dimensional incremental equilibrium equations, i.e. the possibility of the onset of a localized deformation band in three-dimensions. The corresponding load parameter λ for each point on the dashed curve is the lowest load parameter at which $L_{ijkl}(\lambda)n_j n_l$ loses positive definiteness on the radial loading path in question. According to the general theory presented in Section 2, we seek surface bifurcations in the elliptic regime of the material, which explains why the surface bifurcation curves are entirely inside the loss of ellipticity curves. For comparison purposes we also plot by a dotted curve, in the same figures, the forming limit curve which corresponds to the onset of localized necking in a biaxially stretched thin sheet. The corresponding load parameter λ for each point on the dotted curve is the lowest load parameter at which $P_{\alpha\beta\gamma\delta}(\lambda)n_\beta n_\delta$ loses positive definiteness on the radial loading path in question, where the plane stress incremental moduli $\mathbf{P}(\lambda)$ are derived from their three-dimensional counterpart $\mathbf{L}(\lambda)$ by

$$P_{\alpha\beta\gamma\delta} = L_{\alpha\beta\gamma\delta} - \frac{L_{\alpha\beta 33}L_{33\gamma\delta}}{L_{3333}}. \tag{25}$$

The forming limit curves are meaningful for tensile principal stresses and hence are plotted only for $\sigma_1 > 0$ and $\sigma_2 > 0$. It should be remarked here that the plotting of the forming limit curve in the principal strain space is a popular tool for assessing the formability of alloys in sheet metal forming industry and the corresponding diagrams, termed forming limit diagrams (FLD) have been produced experimentally and predicted analytically for an infinite variety of alloys (see discussion in Stören and Rice (1975)).

The results in Figures 2-4 correspond to straining paths with the principal axes oriented at $\alpha = 0$, $\pi/6$ and $\pi/4$ respectively to the rolling direction of the alloy. It should be mentioned here that due to the orthotropy of the material the results are symmetric about $\alpha = \pi/4$. For the principal strains of the same sign $\varepsilon_1\varepsilon_2 > 0$ (first and fourth quadrant of the graphs) the effects of the change of the orientation angle α are not that pronounced, i.e. the forming limit, surface instability and loss of three-dimensional ellipticity results never differ by more than 12%, between the three different values of α, except in a small region near $\varphi = \pi/18$. Notice the discontinuity in the slope of the curves for $\varphi = \pi/18$ when

$\alpha = 0$ and for $\varphi = \pi/4,\ 5\pi/4$ when $\alpha = \pi/6,\ \pi/4$. For $\varepsilon_1 = \varepsilon_2$ ($\varphi = \pi/4,\ 5\pi/4$), the forming limit, surface instability and loss of ellipticity curves in Figures 2-4 all coincide respectively, as expected from the resulting isotropic strain state.

The influence of the orientation angle α is considerably more pronounced in the case of the principal strains of a different sign $\varepsilon_1\varepsilon_2 < 0$ (second and fourth quadrant of the graphs). The biggest changes, for the different orientation angles, occur in the neighborhood of $\varphi = 3\pi/4,\ 7\pi/4$. Notice in particular the changes in the critical surface strains between $\alpha = \pi/6$ and $\alpha = \pi/4$, which can differ by up to 83% between the two cases. It should also be remarked that unlike the case of the principal strains of the same sign, for certain strain paths with $\varepsilon_1\varepsilon_2 < 0$ the loss of ellipticity and surface instability curves coincide, i.e. there is no surface instability in the elliptic regime of the material response.

A typical graph for the orientation angle of the surface mode Ω_c as a function of the load path angle φ is depicted by a solid line in Figure 5 and corresponds to the principal strains oriented at $\alpha = \pi/6$ with respect to the rolling direction. On the same graph is also plotted in a dashed line the orientation angle θ of the principal stresses corresponding to the onset of the surface bifurcation and the forming limit curve, since the orientation of the principal stresses remains almost constant during a proportional straining path. The orientation angle of the localized failure zone corresponding to the forming limit curve ψ_c is plotted in a dotted line for $\sigma_1 > 0$ and $\sigma_2 > 0$. It is interesting to note that the orientation angles Ω_c and ψ_c do not coincide, but are close for positive principal strains, and are both different from the principal stress orientation angle θ. The two curves for θ as a function of φ are due to the fact that one corresponds to σ_1 and the other to σ_2. It is also worth mentioning that for each load orientation angle φ there is only one value of Ω_c and ψ_c with the obvious exception of the hydrostatic straining at $\varphi = \pi/4,\ 5\pi/4$, due to symmetry, and near three of the four locations of the change of sign in the principal stresses.

All of the above reported calculations correspond to a 2024-T3 anisotropic aluminum alloy with a yield surface exponent $m = 8$. The influence of the anisotropy and the yield surface exponent m on the surface bifurcation curves is investigated in Figure 6, which depicts the surface bifurcation results for the 2024-T3 alloy plus two additional hypothetical comparison materials. An isotropic solid $c_J = 1$ with the same yield surface exponent $m = 8$ as the actual 2024-T3 alloy and a J_2 isotropic material $c_J = 1$ with $m = 2$ which only shares the same uniaxial stress-strain curve as the actual alloy for $\alpha = 0$. Notice the significant influence of m which results in a consistent over-prediction of surface bifurcation by the isotropic J_2 deformation theory by as much as 30% for the isotropic straining case. In comparing the $m = 8$ isotropic to the anisotropic cases the changes are not monotonic. In addition to the expected differences between the critical strain predictions for principal strains of the opposite sign, notice the significant differences (maximized for $\varphi = \pi/4$) in the predictions of the two different isotropic comparison solids for principal

strains of the same sign. The latter observation indicates that the correct yield surface characterization is more important for the prediction of surface bifurcation than the anisotropy for the same sign principal strains.

5 Conclusion

The development of strain induced surface roughness is an important factor which limits formability of alloys with a desired high quality surface finish. For small strains, the development of surface roughness is due to the surface grain misorientation and appears in the form of random "*orange peel*". This effect can be reduced by surface treatment which results in the smaller grain size. Surface roughness for large strains, which appears in the form of same orientation wavelets several grains wide, is a surface bifurcation instability due to the nonlinear kinematics and the constitutive response of the solid. This instability is inevitable at high strains and is a precursor to the ultimate fracture failure of the material. Unlike the previous phenomenon, it is amenable to a continuum description which admits analytical solutions for the case of a half-space idealization.

Surface bifurcation is extremely sensitive to the constitutive description of the material. Past work was available only for the von Mises type isotropic materials, thus motivating the present study on the influence of anisotropy on surface bifurcation. The present calculations for an actual aluminum alloy, although indicative due to the extreme difficulty in obtaining experimental verification, show that anisotropy is extremely important for the case of principal strains of the opposite sign. Moreover, it is also found that the yield surface characterization plays an important role near balanced biaxial strains.

The above proposed continuum approach can be improved by the incorporation of grain size effects to predict the characteristic length of the surface mode. Improvements on the continuum approach always provide an analytically tractable alternative to the full scale micromechanical calculations in three-dimensions which involve fine meshing of many grains.

ACKNOWLEDGMENTS

The partial support of ALCOA and NSF under grant G-CMS-9503956 are gratefully acknowledged.

References

[1] Barlat, F., Lege, D. J. and Brem, J. C. (1991) A Six-Component Yield Function for Anisotropic Materials, *Int. J. Plasticity*, **7**, 693–712.

[2] Becker, R. (1997) Effects of Strain Localization on Surface Roughening During Sheet Forming, to appear in *Acta Materialia*.

[3] Biot, M. A. (1965) *Mechanics of Incremental Deformations*, Wiley, New York.

[4] Hershey, A. V. (1954) The Plasticity of an Isotropic Aggregate of Anisotropic Face Centered Cubic Crystals, *J. Appl. Mech. Trans. ASME*, **21**, 241–249.

[5] Hill, R. (1950) *The Mathematical Theory of Plasticity*, Clarendon Press, Oxford.

[6] Hill, R. and Hutchinson, J. W. (1975) Bifurcation Phenomena in the Plane Tension Test, *J. Mech. Phys. Solids*, **23**, 239–264.

[7] Hutchinson, J. W. (1974) Plastic Buckling, *Adv. Appl. Mechanics*, **14**, 67–144.

[8] Hutchinson, J. W. and Tvergaard, V. (1980) Surface Instabilities on Statically Strained Plastic Solids, *Int. J. Mech. Sciences*, **22**, 339–354.

[9] Karafillis, A. P. and Boyce, M. C. (1993) A General Anisotropic Yield Criterion Using Bounds and a Transformation Weighting Tensor, *J. Mech. Phys. Solids*, **41**, 1859–1886.

[10] Larsson, M., Needleman, A., Tvergaard, V. and Storakers, B. (1982) Instability and Failure of Internally Pressurized Ductile Metal Cylinders, *J. Mech. Phys. Solids*, **30**, 121–154.

[11] Rice, J. R. (1976) The Localization of Plastic Deformation, *Theoretical and Applied Mechanics*, W. T. Koiter, editor, 207–220, proceedings of the 14*th* IUTAM Congress, Delft, Netherlands.

[12] Stören, S. and Rice, J. R. (1975) Localized Necking in Thin Sheets, *J. Mech. Phys. Solids*, **23**, 421–441.

[13] Triantafyllidis, N. (1980) Bifurcation Phenomena in Pure Bending, *J. Mech. Phys. Solids*, **28**, 221–245.

[14] Triantafyllidis, N. (1984) Surface Instabilities in Finitely Strained Solids Under Static Loading, *Int. J. Eng. Science*, **22**, 1187–1192.

[15] Triantafyllidis, N. and Needleman, A. (1980) Analysis of Wrinkling in the Swift Cup Test, *J. Eng. Mater. Technol. Trans. ASME*, **102**, 241–248.

[16] Triantafyllidis, N., Needleman, A. and Tvergaard, V. (1982) On the Development of Shear Bands in Pure Bending, *Int. J. Solids Structures*, **18**, 121–138.

[17] Young, N. J. B. (1976) Bifurcation Phenomena in the Plane Compression Test, *J. Mech. Phys. Solids*, **24**, 77–91.

FIGURE CAPTIONS

Figure 1: Schematic representation of the half-space indicating orientation angle Ω_c of the surface mode.

Figure 2: Surface bifurcation depicted by a solid line, three-dimensional loss of ellipticity and forming limit curves depicted by a dashed and a dotted line respectively, are plotted in principal strain space for a 2024-T3 aluminum alloy strained at an angle $\alpha = 0$ with respect to its rolling direction.

Figure 3: Surface bifurcation depicted by a solid line, three-dimensional loss of ellipticity and forming limit curves depicted by a dashed and a dotted line respectively, are plotted in principal strain space for a 2024-T3 aluminum alloy strained at an angle $\alpha = \pi/6$ with respect to its rolling direction.

Figure 4: Surface bifurcation depicted by a solid line, three-dimensional loss of ellipticity and forming limit curves depicted by a dashed and a dotted line respectively, are plotted in principal strain space for a 2024-T3 aluminum alloy strained at an angle $\alpha = \pi/4$ with respect to its rolling direction.

Figure 5: Orientation angle Ω_c for the onset of surface bifurcation depicted by a solid line and angle ψ_c for the onset of plane stress necking, i.e. forming limit, depicted by a dotted line, are plotted as functions of the principal strain ratio angle φ. The principal stress orientation angle θ which is essentially constant during proportional straining is plotted in a dashed line.

Figure 6: Surface bifurcation curves plotted by solid lines in principal strain space for a 2024-T3 aluminum alloy strained at $\alpha = 0, \pi/6$ and $\pi/4$ with respect to its rolling direction. For comparison purposes, surface bifurcation of two isotropic materials with the same uniaxial stress-strain curve as the actual alloy for $\alpha = 0$ are also plotted. The dotted curve corresponds to the finite strain generalization of J_2 deformation theory of plasticity while the dashed curve corresponds to an isotropic material which shares the same yields surface with the actual alloy.

FIGURES

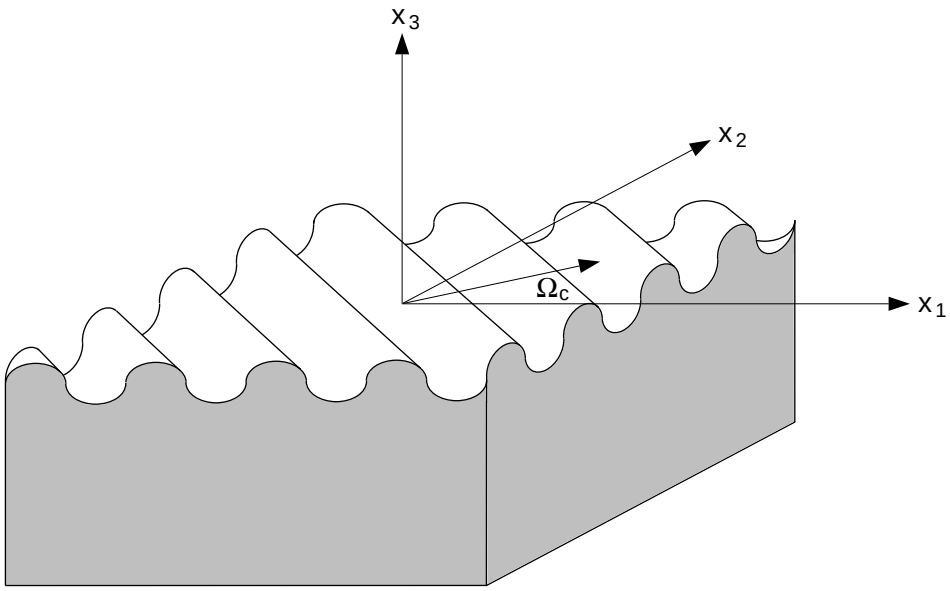

Figure 1: See FIGURE CAPTIONS

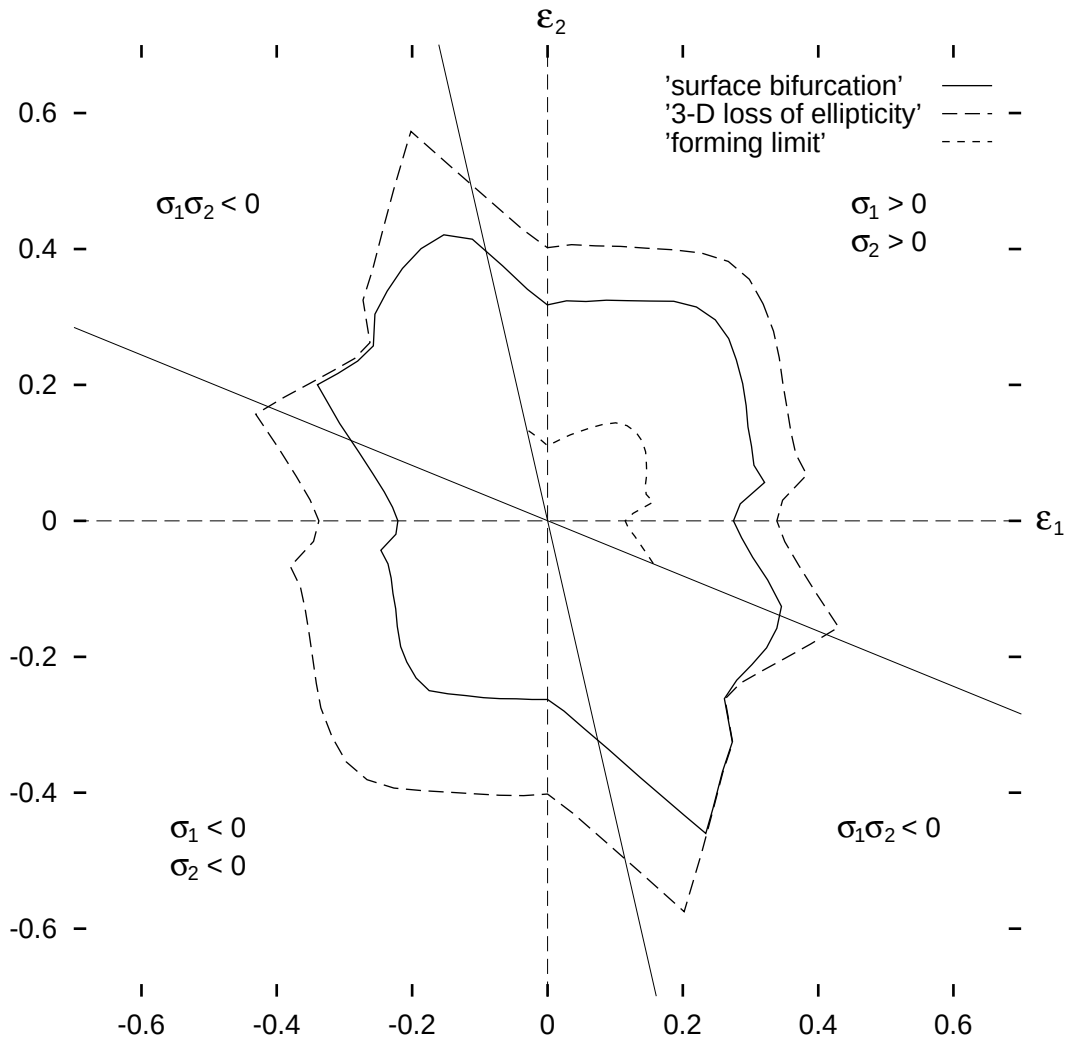

Figure 2: See FIGURE CAPTIONS

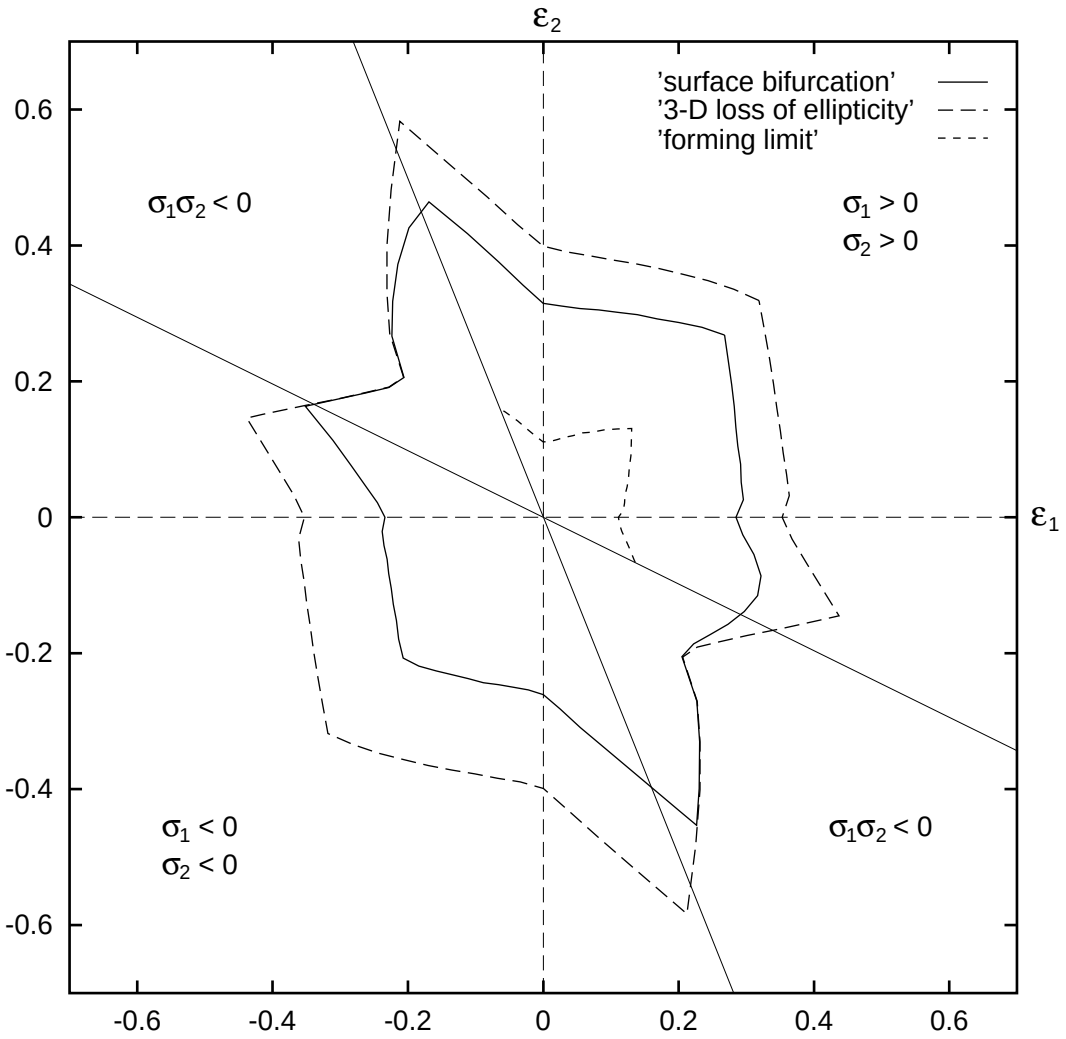

Figure 3: See FIGURE CAPTIONS

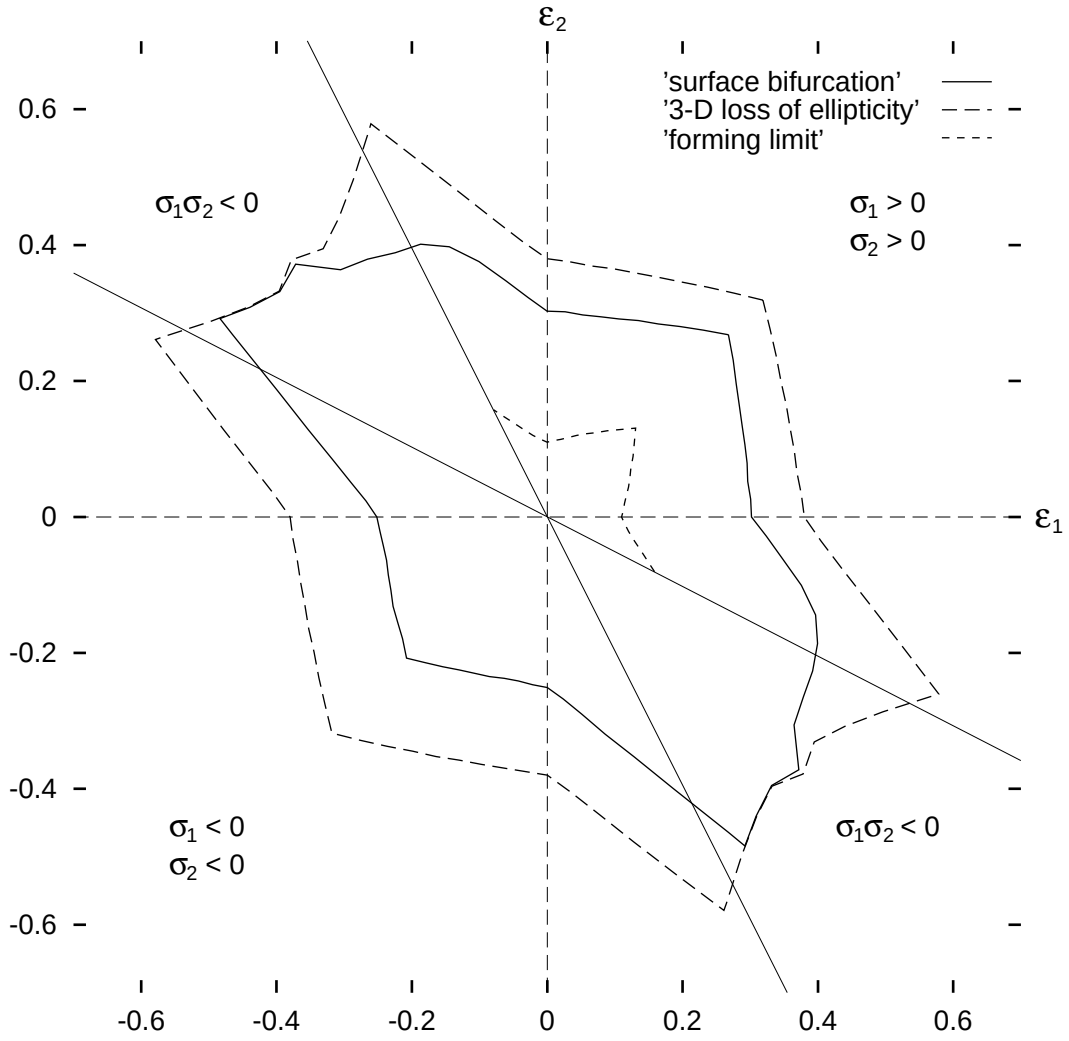

Figure 4: See FIGURE CAPTIONS

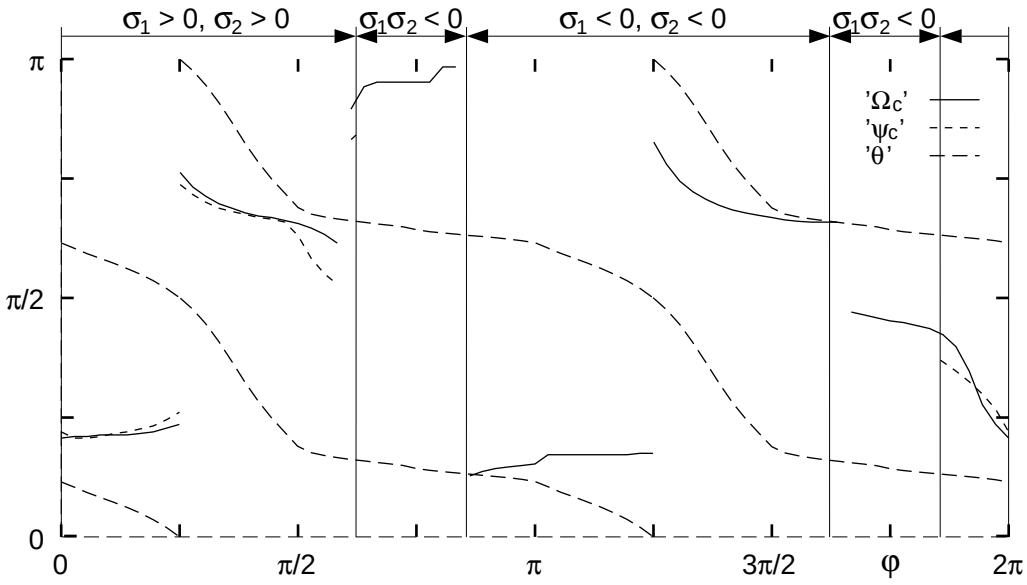

Figure 5: See FIGURE CAPTIONS

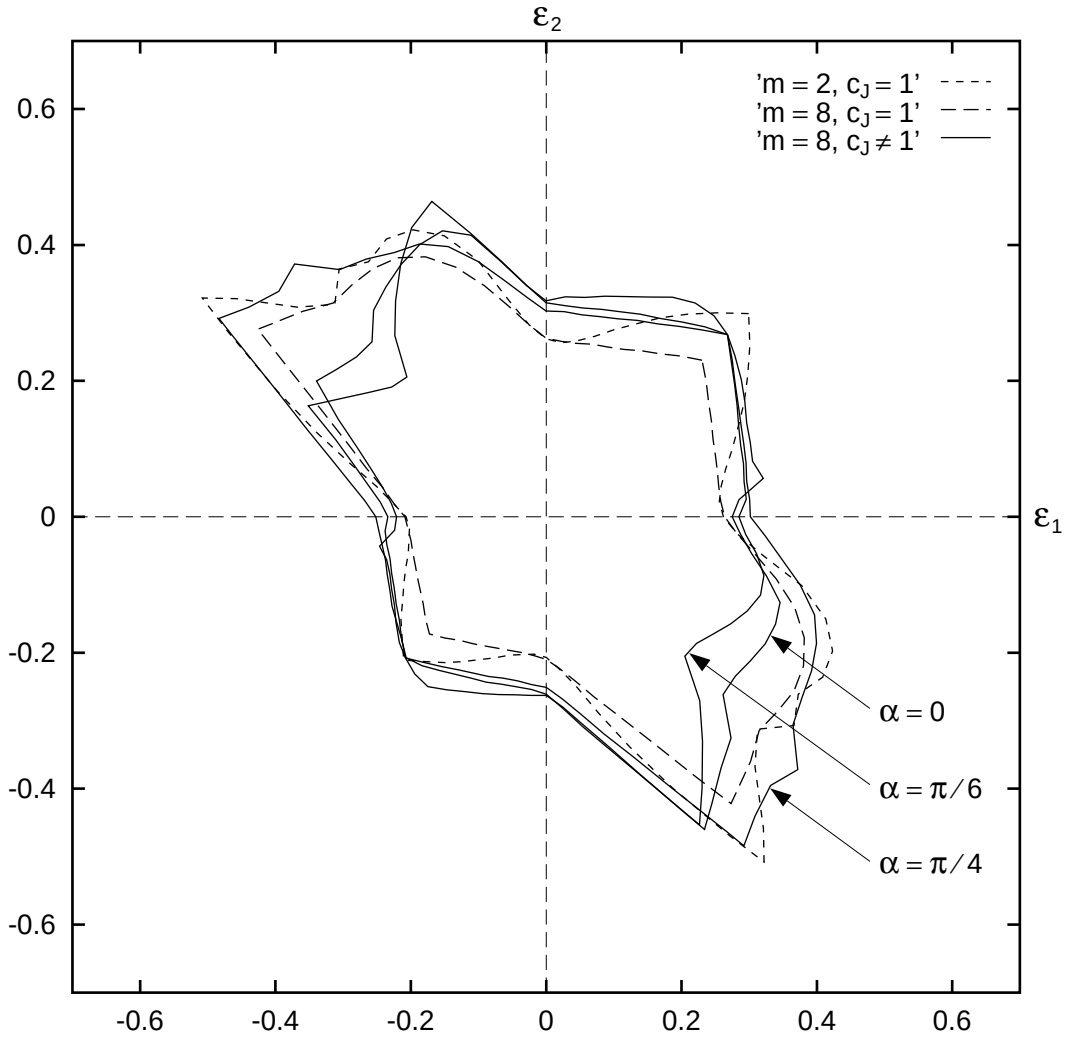

Figure 6: See FIGURE CAPTIONS